

# Hybrid Quantum–Classical Machine Learning Potential with Variational Quantum Circuits

Soohaeng Yoo Willow,<sup>1</sup> David ChangMo Yang,<sup>1</sup> and Chang Woo Myung<sup>1,2,3,\*</sup>

<sup>1</sup>*Department of Energy Science, Sungkyunkwan University,  
Seobu-ro 2066, Suwon, 16419, Korea*

<sup>2</sup>*Department of Energy, Sungkyunkwan University,  
Seobu-ro 2066, Suwon, 16419, Korea*

<sup>3</sup>*Department of Quantum Information Engineering,  
Sungkyunkwan University, Seobu-ro 2066, Suwon, 16419, Korea*

(Dated: August 6, 2025)

## Abstract

Quantum algorithms for simulating large and complex molecular systems are still in their infancy, and surpassing state-of-the-art classical techniques remains an ever-receding goal post. A promising avenue of inquiry in the meanwhile is to seek practical advantages through hybrid quantum-classical algorithms, which combine conventional neural networks with variational quantum circuits (VQCs) running on today’s noisy intermediate-scale quantum (NISQ) hardware. Such hybrids are well suited to NISQ hardware. The classical processor performs the bulk of the computation, while the quantum processor executes targeted sub-tasks that supply additional non-linearity and expressivity. Here, we benchmark a purely classical  $E(3)$ -equivariant message-passing machine learning potential (MLP) against a hybrid quantum-classical MLP for predicting density functional theory (DFT) properties of liquid silicon. In our hybrid architecture, every readout in the message-passing layers is replaced by a VQC. Molecular dynamics simulations driven by the HQC-MLP reveal that an accurate reproduction of high-temperature structural and thermodynamic properties is achieved with VQCs. These findings demonstrate a concrete scenario in which NISQ-compatible HQC algorithm could deliver a measurable benefit over the best available classical alternative, suggesting a viable pathway toward near-term quantum advantage in materials modeling.

---

\* [cwmyung@skku.edu](mailto:cwmyung@skku.edu)

## I. Introduction

Quantum Machine Learning (QML) has emerged as a significant research frontier, aiming to integrate the principles of quantum computation with the adaptive frameworks of machine learning. The central premise of QML is its potential to leverage quantum phenomena, such as superposition and entanglement, to process information in high-dimensional Hilbert spaces. This capability is theorized to offer substantial advantages over classical models for tasks involving intricate data correlations, leading to active investigation into its application for optimization, classification, sampling techniques, and molecular modeling [1–8].

However, despite the growing enthusiasm surrounding QML, there is also skepticism about its practical utility, especially in the near term. Many quantum models have struggled to outperform their classical counterparts in key areas, and the exact role of “quantumness” in improving performance remains an open question. Studies have shown that while quantum circuits can represent certain nonlinear relationships more efficiently, the inductive bias provided by quantum systems and the problems for which they are particularly well suited are still not fully understood [9]. Classical baseline models outperform prototypical quantum models in small-scale benchmark datasets and no clear advantage of quantum entanglement in QML was found [9]. As such, QML research remains in a stage of exploration, with both its potential and limitations yet to be fully defined.

One of the most compelling and underexplored of these domains is the development of machine learning potentials (MLPs) for materials science [10–19]. This field is particularly suitable for quantum approaches because the underlying atoms and molecules being modeled are inherently quantum mechanical. The main challenge in this area has always been the rather unfavorable computational cost of traditional *ab initio* methods like density functional theory (DFT), Møller-Plesset (MP) perturbation theory, and coupled cluster (CC) theory. In particular, the conventional DFT method scales with the system size  $N$  as  $\mathcal{O}(N^3)$ , while second-order MP theory (MP2) and CC theory with single, double, and perturbative triple excitations [CCSD(T)] scale steeply as  $\mathcal{O}(N^5)$  and  $\mathcal{O}(N^7)$ , respectively. As capable as the latter methods are of capturing complex quantum mechanical correlations for accurate description of molecular systems, their scaling laws render large-scale simulations intractable. To address this scaling problem, classical MLPs have emerged as a revolutionary tool over the past two decades, capable of learning the complex potential energy surface from refer-

ence *ab initio* calculations, enabling simulations with near-quantum accuracy at a fraction of the computational cost. The field has seen rapid progress, evolving from architectures like feed-forward neural networks [20, 21] and Gaussian Approximation Potentials [22–31] to the current state-of-the-art  $E(3)$ -equivariant graph neural networks, which respect the fundamental symmetries of physics [32–35]. Despite their remarkable success in enabling large-scale materials simulations, these classical models are not without their own limitations. Their accuracy is highly dependent on extensive, computationally expensive training datasets, and they still face challenges in capturing the non-local correlations present in complex systems. This creates a clear and compelling opportunity to investigate whether the integration of QML can push the boundaries of what is possible in atomistic modeling.

The potential for quantum advantage in QML is often linked to the ability to recognize hidden patterns in quantum data. Non-local quantum measurements can extract underlying parameters from quantum datasets using only a few samples [36]. In the context of applying QML to MLPs, referred to as quantum MLPs (QMLPs), the primary goal is to demonstrate quantum advantage by surpassing the performance of classical state-of-the-art MLP models. However, the challenge arises from the fact that the local chemical environment, which is inherently classical, must be mapped onto qubits. This poses a disadvantage, as no known quantum speedup exists for such classical-to-quantum data transformations [37–39]. Despite this challenge, several studies suggest that polynomial advantage may still be possible for purely classical problems using quantum algorithms [36, 40–43]. However, a clear understanding of how quantum advantage would manifest itself in classical tasks such as QMLP has yet to emerge. For this reason, it is crucial to investigate potential quantum advantages in two key areas: data embedding and the variational Ansatz. When classical local chemical environments are embedded into qubits, the effectiveness of the embedding scheme becomes critical. Furthermore, understanding whether exploiting quantum entanglement can improve machine learning performance during training is another essential aspect. The construction of an effective variational Ansatz circuit with activation functions for potential energy and force regression is crucial for exploring the quantum advantage in QMLPs [44]. Building an equivariant QNN is also important for probing the quantum advantage in QMLPs [9, 38]. These aspects require careful consideration to elucidate how quantum resources may offer tangible benefits over classical approaches.

In contrast to the considerable attention QML has received in other fields, its application

to MLPs in materials science remains largely unexplored. Given the quantum nature of the systems being modeled, there is an untapped potential for QMLPs to enhance the efficiency and accuracy of MLPs. The hybrid quantum-classical MLP (HQC-MLP), which combines the strengths of quantum and classical computing, is particularly well suited for this task. HQC-MLP leverages the processing power of quantum circuits while utilizing the stability and scalability of classical models, offering a balanced approach that can take advantage of current quantum hardware without full quantum encoding of material descriptors [1, 2].

Here, we develop HQC-MLP methods and apply them for the simulation of molecular dynamics (MD) of liquid silicon at a computationally frequented [45–47] temperature of 2000 K and an unreported temperature of 3000 K. Our HQC-MLP models are trained with the results from *ab initio* MD (AIMD) simulation of liquid silicon. The classical processor performs the bulk of the computation, while the quantum processor executes targeted sub-tasks that supply additional non-linearity and expressivity. We find that this hybrid approach not only accelerates the training process, but also achieves predictive accuracy comparable to purely classical models, suggesting that HQC-MLP holds significant potential for advancing the field of materials science through the efficient modeling of complex atomistic systems.

## II. Hybrid quantum-classical machine learning potential

The objective of our model is to learn a mapping from the positions  $\{\mathbf{r}_i\}$  and chemical species  $\{Z_i\}$  of the  $i$ -th atom of a system to its total potential energy

$$E_{\text{pot}} = \sum_i^{N_{\text{atoms}}} \sum_t^{N_{\text{layers}}} E_i^{(t)} = \sum_i^{N_{\text{atoms}}} E_i \quad (1)$$

and the corresponding atomic forces  $\mathbf{f}_i = -\nabla_i E_{\text{pot}}$ . The model is designed to be energy-conserving by the definition of forces as the negative gradient of the potential energy.

The total potential energy is decomposed into the sum of local atomic contributions  $E_i = \sum_t^{N_{\text{layers}}} E_i^{(t)}$ . Crucially, the model must adhere to physical symmetries:  $E_{\text{pot}}$  must be invariant under translations, rotations, and reflections of the system, while vector quantities like forces and internal geometric features must be correspondingly equivariant.

The architecture of our HQC-MLP (Figure 1) is based on an  $E(3)$ -equivariant message

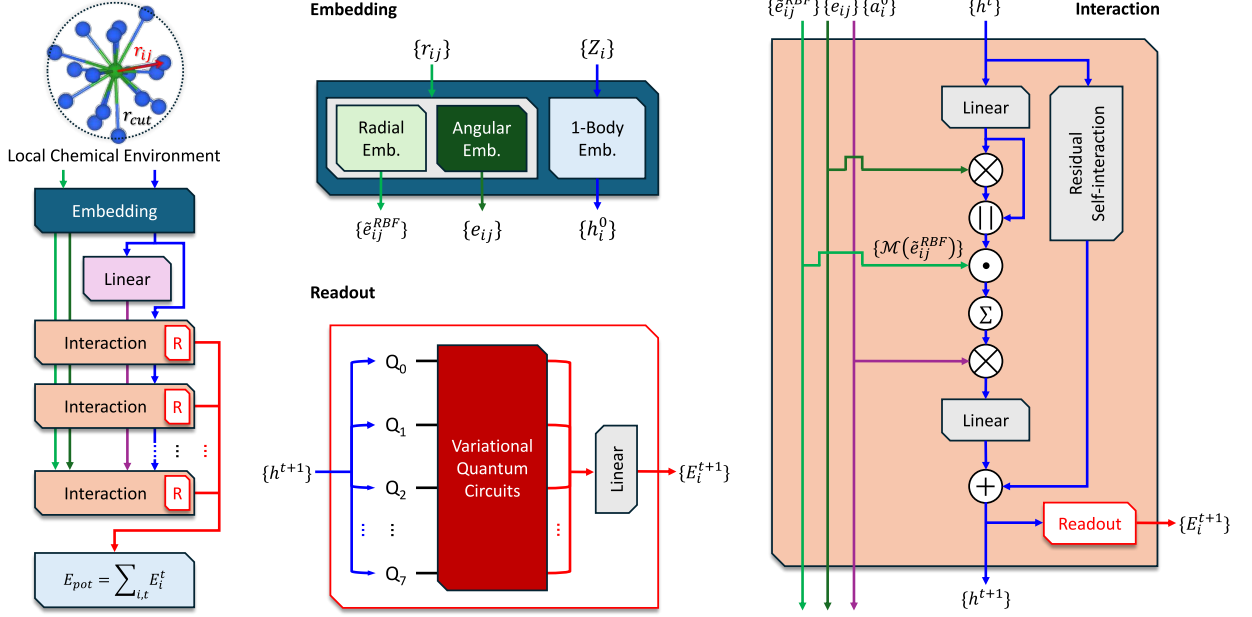


FIG. 1. Architecture of the hybrid quantum-classical machine learning potential (HQC-MLP). The HQC-MLP model consists of an embedding layer and interaction layers. Each interaction layer includes a readout layer that predicts output values. In the embedding layer, node features ( $h_i$ ) are initialized based on the atomic numbers of the nodes  $\{Z_i\}$ , while edge features  $e_{ij}$  and radial basis vectors  $\tilde{e}_{ij}^{\text{RBF}}$  are assigned based on pairwise vectors  $\mathbf{r}_{ij} = \mathbf{r}_j - \mathbf{r}_i$ . The interaction layer updates node features in a RESNET-like scheme. The readout layer applies a nonlinear transformation to the node features, generating output values that represent the energy value associated with each node. In the HQC-MLP model, variational quantum circuits VQC, executing nonlinear transformations [2, 3]. It includes a feature map module, which takes the node features as input, and an Ansatz module, which contains trainable parameters  $\theta$ . Five different VQC Ansatz modules in Figure 2 were tested.

passing neural network (MPNN). In this framework, each atomic structure is converted into a graph where atoms are nodes and the edges connect neighbors within a cutoff radius  $r_{\text{cut}}$ . MPNN iteratively updates the node features through message-passing operations. To ensure the required symmetries, the message-passing convolutions employ steerable filters,  $S(\mathbf{r}_{ij})$ , constructed from products of learnable radial functions  $R(r_{ij})$  and spherical harmonics  $Y_m^{(l)}(\hat{\mathbf{r}}_{ij})$ :

$$S_m^{(l)}(\mathbf{r}_{ij}) = R^{(l)}(r_{ij})Y_m^{(l)}(\hat{\mathbf{r}}_{ij}) \quad (2)$$

where  $\mathbf{r}_{ij} = \mathbf{r}_j - \mathbf{r}_i$  are the pairwise relative interatomic coordinates which can be represented by distances  $r_{ij}$  and unit directional vectors  $\hat{\mathbf{r}}_{ij}$ . The irrep index ( $l$ ), also known as the

angular momentum quantum number, is understood as the layer index. This construction makes the filters, and consequently the network features, equivariant under  $SO(3)$  rotations.

The features of the atoms are represented as learnable node features ( $h_i^{(t)} \in \mathbb{R}^F$ ), where  $F$  represents the dimension of the node features and  $(t)$  is the index of the (composite) interaction layer. The features of the initial node  $h_i^{(0)}$  are determined based on an embedding related to the atomic numbers  $\{Z_i\}$  as  $h_i^{(0)} = \mathbf{a}_{Z_i}$ , where the atomic-type embeddings  $\mathbf{a}_Z$  are randomly initialized and then optimized during the training process.

The radial basis vectors  $\tilde{e}_{ij}^{\text{RBF}} \in \mathbb{R}^{N_{\text{RBF}}}$  for the interatomic distance [48] are defined by Bessel basis functions  $B_n(x) = \sqrt{\frac{2}{r_c^3} \frac{j_0(n\pi x)}{|j_1(n\pi)|}}$  and a polynomial envelope function  $f_{\text{env}}$  as

$$\tilde{e}_{\text{RBF}}(r_{ij}) = B_n(r_{ij}/r_c) f_{\text{env}}(r_{ij}, r_c). \quad (3)$$

Here,  $j_0$  and  $j_1$  are spherical Bessel functions of the first kind. The edge features  $e_{ij}$  encode the direction information and are obtained as  $Y_m^{(l)}(\hat{r}_{ij})$ .

The goal of the interaction layer is to update the node energy value by incorporating the effects of edge interactions, including the bond and dispersion energies. To achieve this, the node features are updated in the scheme of RESNET [49]:

$$\mathbf{h}^{(t+1)} = f_{\text{SI}}(\mathbf{h}^{(t)}) + f(\mathbf{h}^{(t)}, \mathbf{e}_{ij}, \tilde{e}_{ij}^{\text{RBF}}). \quad (4)$$

Here,  $f$  represents a sequence of an atom-wise dense layer  $f_{\text{dense}}$ , an interatomic continuous-filter convolution layer  $f_{\text{conv}}$ , and two additional atom-wise dense layers. The weights in the self-interaction layer  $f_{\text{SI}}$  are learned separately for each atomic number.

In the convolution layer  $f_{\text{conv}}$ , the node features are updated according to

$$h_i = \sum_{j \in N_i} [(e_{ij} \otimes h_j) \odot \mathcal{M}(\tilde{e}_{ij}^{\text{RBF}})] \quad (5)$$

where  $\otimes$  denotes the rotationally equivariant tensor product (as detailed in the Supporting Information, Eq. S1) and  $\odot$  refers to the element-wise multiplication. A multilayer perceptron  $\mathcal{M}$  is applied to the radial basis vectors  $\tilde{e}_{ij}^{\text{RBF}}$  to capture interatomic interactions based on distance. As a result,  $\mathcal{M}(\tilde{e}_{ij}^{\text{RBF}})$  encodes the learnable radial functions  $R^{(t)}(r_{ij})$  in Eq. 2. Finally, the convolution filters  $S_m^{(t)}$  in Eq. 2 are encoded through the convolution layer  $f_{\text{conv}}$  within the models.

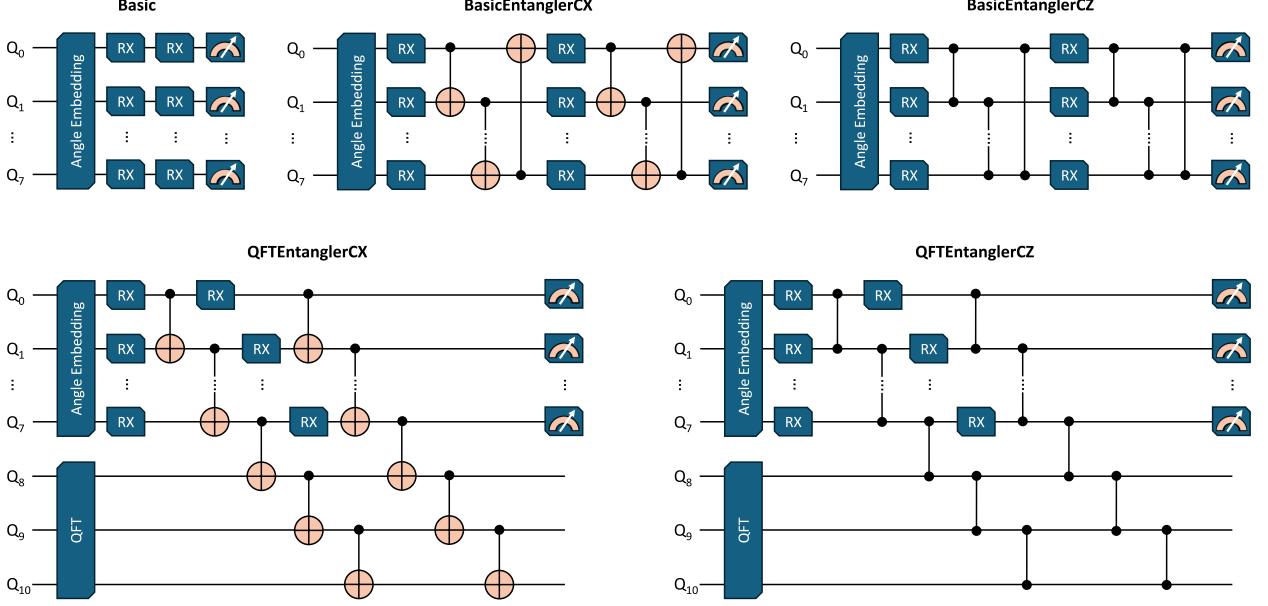


FIG. 2. Diagrams of five distinct Ansatz modules with 8 qubits for `AngleEmbedding`, 3 qubits for `QFT`, and 2 layers for trainable rotational gates `RX`. The `AngleEmbedding` module served as the feature map across all quantum circuits, each using one of five Ansatz module variations. These Ansatz modules are categorized based on the type of the entanglement and whether quantum Fourier transform (`QFT`) is incorporated. Entanglement between qubits is achieved using either the controlled-NOT (`CX`) or the controlled-Z (`CZ`). All Ansatz modules have three layers.

To calculate the energy value  $E_i^{(t)}$  of node  $i$  from its feature at the  $t$ -th interaction layer, the invariant part of the node feature is mapped to the node energy via the readout function:

$$E_i^{(t)} = \sum_{\tilde{k}} W_{\tilde{k}}^{(t)} (h_{i,\tilde{k}}^{(t)}), \quad (6)$$

where  $W_{\tilde{k}}^{(t)}$  represents the readout weights, and  $h_{i,\tilde{k}}^{(t)}$  represents the  $\tilde{k}$ -th element of the  $i$ -th node feature at the current layer ( $t$ ). To ensure invariance of the node energy  $E_i^{(t)}$ , the readout layer is only based on the invariant features (those with rotational order of  $l = 0$ ). These features are obtained by applying the transformation  $h_i^{(t)} = \text{Gate}(f_{\text{dense}}^{l=0}(h_i^{(t)}))$ , where  $\text{Gate}(\cdot)$  refers to an equivariant `SiLU`-based gate in the MLP on classical computers. In our HQC-MLP model, we replace this classical readout part with variational quantum circuits (VQCs). The invariant feature vector of the classical neural network is used as input to parameterize the VQCs. The circuit's output is interpreted as the local energy  $E_i^{(t)}$ . This substitution allows a quantum processor to handle the final nonlinear mapping from the learned latent features to local energy, representing the core of our hybrid approach.

The VQC module is designed to map the classical input features to the final energy contribution and consists of three stages: feature encoding, a variational Ansatz, and measurement. First, the invariant node features from the message-passing,  $h_{i,\bar{k}}^{(t)}$ , are encoded onto an  $N$ -qubit state using an angle embedding scheme. Each element of the feature vector is used to parameterize a single-qubit rotation gate (e.g. RY gates), which prepares the initial state for the variational circuit. The core of the VQC is the parameterized Ansatz, which performs a nonlinear transformation on the encoded state. To systematically study the impact of circuit structure on model performance, we designed and tested five Ansatz architectures (Figure 2). These architectures are differentiated by their primary components, specifically the type of entangling gates used (CX vs. CZ) and the optional inclusion of a quantum Fourier transform (QFT) block. For instance, we designed a baseline circuit with a simplified structure in order to isolate the effect of entanglement, which is a key aspect of “quantumness”. Each Ansatz was constructed with three repeated layers, a depth found to be effective in related QML applications [4]. The trainable parameters of the Ansatz are optimized concurrently with the classical components of the model. Finally, the energy contribution is extracted by measuring the expectation value of the Pauli  $Z$  observable. All quantum circuits were implemented using the PENNYLANE software library [50]. Our simulations were conducted using a total of 8 qubits for the main circuit, with the QFT module, when present, acting on an additional 3-qubit subsystem.

### III. Results and discussion

#### III.1. Training of HQC-MLP models

To evaluate the models, we generated a dataset of 1,000 liquid silicon configurations at 3000 K from Born–Oppenheimer molecular dynamics (BOMD) simulations using DFT. This was partitioned into 900+50+50 configurations for training, validation, and test, respectively. Figure 3 compares the training and validation loss curves for the CMLP and the HQC-MLP models.

A significant challenge for scaling VQCs is the issue of barren plateaus (BPs) — the exponential vanishing of gradients during training [51]. This phenomenon is attributed to several factors, including high circuit expressivity, the use of global loss functions, and, notably, the volume of entanglement in the circuit [52–55]. Although BPs typically manifest

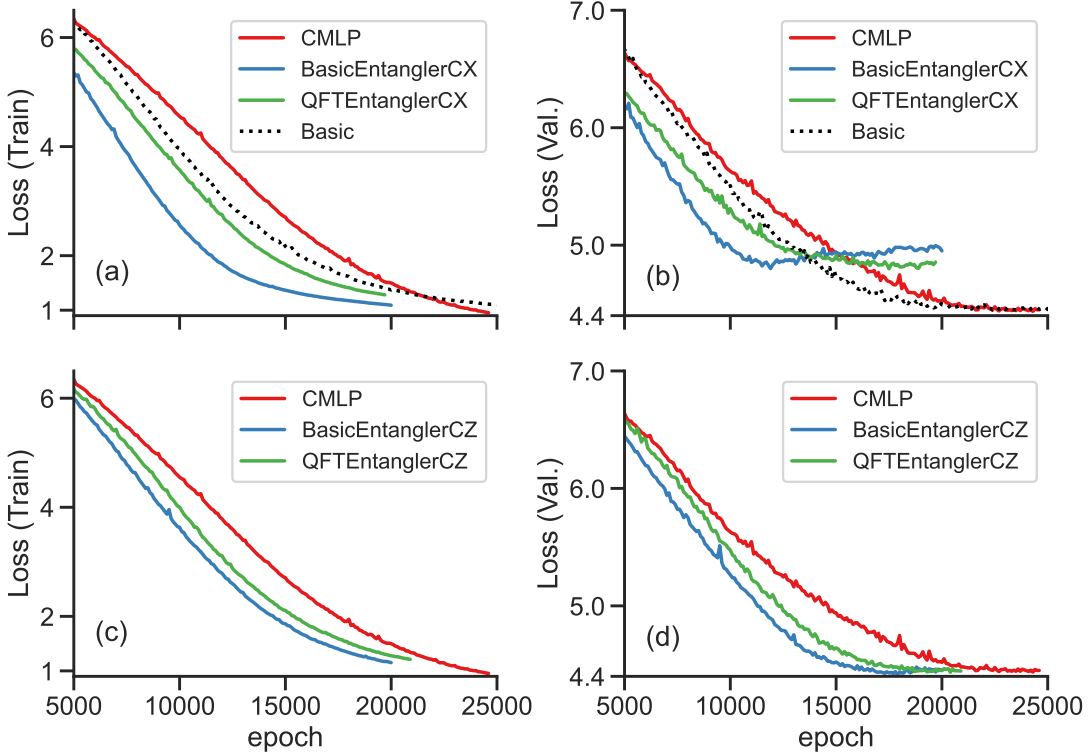


FIG. 3. Loss profiles for hybrid quantum-classical machine learning potential (HQC-MLP) models in comparison to a classical machine learning potential (CMLP) model. Loss values are evaluated for (a, c) training and (b, d) validation datasets. In the training dataset, loss values continue to decrease. In the validation dataset, however, loss values reach minimum points, indicating the onset of model overfitting to the training data.

as failure to train, the associated high expressivity and entanglement can also lead to poor generalization. Figures 3 and S1 show that, compared to the CMLP model, HQC-MLP models which incorporate entanglement exhibit a rapid decrease in training loss followed by an early onset of overfitting.

A primary observation is that the HQC-MLP models consistently converge faster on the training data than the purely classical model. This acceleration is particularly pronounced for models that incorporate entangling gates, such as the controlled-NOT (CX). However, these hybrid models also exhibit an earlier onset of overfitting, indicated by a premature increase in their validation loss. This tendency was evident in the models utilizing CX entanglement. In contrast, the inclusion of a QFT block for 2D rotation equivariant circuit [9] appears to improve generalization, resulting in lower final loss values on the validation set.

These findings suggest that while entanglement — a key aspect of “quantumness” — can accelerate fitting to the training data, other architectural equivariant components like the QFT may be crucial for enhancing the model’s predictive accuracy on unseen data.

Our results reveal a complex interplay between architectural choice and model performance. A consistent advantage across all HQC-MLP models was an accelerated training convergence compared to the state-of-the-art CMLP. However, this speed was often accompanied by a tendency to overfit, motivating a search for the VQC architecture with the best generalization performance. Our investigation into different VQC designs identified the choice of entangling gate as the most critical factor. The models utilizing the controlled- $Z$  (CZ) gate consistently achieved the best performance, yielding the lowest validation loss among all tested architectures. This superior result was robust, holding for both the simple `BasicEntanglerCZ` model and the partially 2D equivariant `QFTEntanglerCZ` model [9]. In contrast, the models based on the CX gate, while also training rapidly, struggled with more severe overfitting. The addition of the QFT block prevented overfitting but did not fully remedy this issue for the CX variants, whose performance remained inferior to the CZ-based circuits. This distinct performance gap suggests that the nature of the entanglement operation is paramount for this task. The CZ gate, which imparts a conditional phase, appears to be a more effective strategy for this regression problem than the state-flipping CX gate. Therefore, while a definitive “quantum advantage” remains an open question, our findings point to two clear conclusions: a practical benefit in training speed for all hybrid models, and a distinct performance advantage achieved by using CZ-based entanglers. This suggests that for this problem, the introduction of entanglement via these circuit designs may hinder generalization more than the partial restoration of symmetry helps. Consequently, future work should explore more structured entanglement strategies, which have been theorized to mitigate BPs [55] and could potentially lead to models that are both expressive and generalizable.

The root mean squared errors (RMSE) for the predicted energies (in meV/atom) and forces (in eV/Å) from the models were estimated using the test dataset, as shown in Figure S2. Both the HQC-MLP and CMLP models produced an RMSE of approximately 2.0 meV per atom for the predicted energies (RMSE<sub>E</sub>). Similarly, the RMSE for the predicted forces (RMSE<sub>F</sub>) was about 0.2 eV/Å. These RMSE values are comparable to the results reported by Behler and Parrinello [20], where RMSE<sub>E</sub> was around 4 meV per atom,

and  $\text{RMSE}_F$  was approximately  $0.2 \text{ eV/\AA}$ .

### III.2. Molecular dynamics simulations of liquid silicon with HQC-MLP models

Simulating liquid silicon at high temperatures is a well-known challenge, as standard empirical potentials like those of Bazant [56], Lenosky [46], and Tersoff [57] are known to inadequately describe its physical properties. DFT, in contrast, provides an accurate reference that agrees well with experimental data [20]. To assess the ability of our HQC-MLP and compare against CMLP models in this demanding regime, we performed 100 ps molecular dynamics (MD) simulations of liquid silicon at  $T = 2000 \text{ K}$ . A crucial first test for any new potential is the conservation of total energy. We confirmed that all tested HQC-MLP and CMLP models were stable, conserving the total energy throughout the full simulation trajectory, which indicates a smooth learned potential energy surface and accurate forces (see Figure S3).

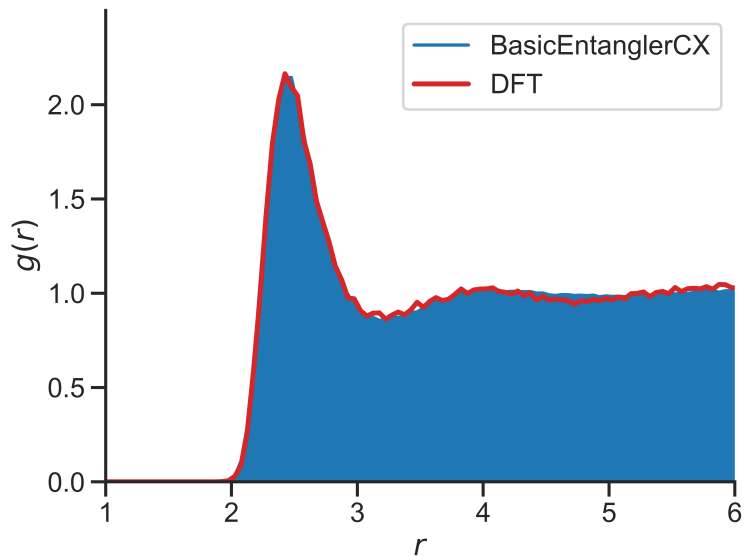


FIG. 4. Radial distribution function,  $g(r)$ , for liquid silicon at  $T = 2000 \text{ K}$ . The plot compares the result from the HQC-MLP(`BasicEntanglerCX`) model (blue filled area) with the reference calculated using DFT (red line), demonstrating excellent agreement. Both curves were obtained from MD simulations of a 64-atom system in a cubic cell ( $a = 10.862 \text{ \AA}$ ).

Figure 4 shows the radial distribution function (RDF) for liquid silicon at  $T = 2000 \text{ K}$ , comparing results from the HQC-MLP(`BasicEntanglerCX`) model with those from the DFT simulations. The DFT-based BOMD simulations were performed for 10 ps to reach equi-

librium, followed by 18 ps for data production. In contrast, MD simulations using the HQC-MLP(BasicEntanglerCX) model were run for 100 ps. The RDF obtained with the HQC-MLP(BasicEntanglerCX) model closely aligned with the RDF produced by the DFT calculations.

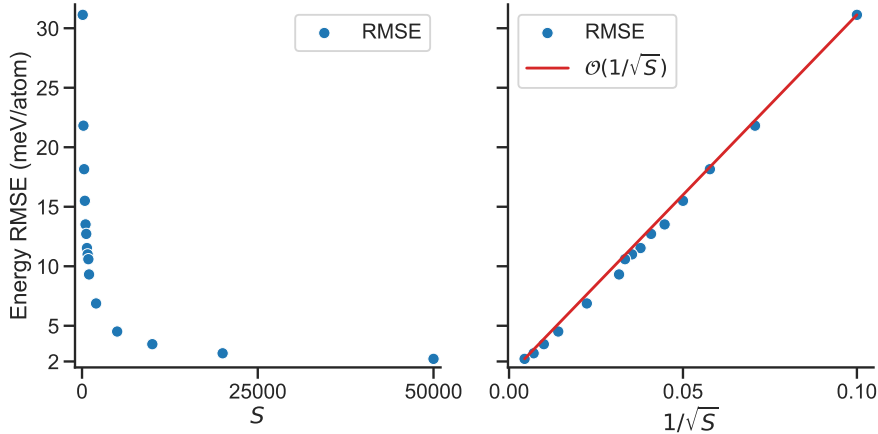


FIG. 5. Dependence of HQC-MLP predictions on the number of measurement shots  $S$ . Root-mean-square-error (RMSE) decreases with  $\mathcal{O}(1/\sqrt{S})$ .

### III.3. Effect of Finite Measurement Shots

The preceding analyses were based on mathematically exact expectation values from the VQCs. To assess the model’s performance in realistic quantum hardware, we investigate the impact of statistical noise arising from a finite number of measurement shots,  $S$ . Figure 5 quantifies the convergence of the predicted potential energies as a function of  $1/\sqrt{S}$ . As expected from sampling theory, the root mean square error (RMSE) between the shot-based predictions and the exact expectation values scales as  $\mathcal{O}(1/\sqrt{S})$ . We determined that achieving an RMSE of approximately 2.0 meV/atom requires on the order of  $5 \times 10^4$  measurement shots per energy evaluation.

A critical consequence of using finite measurement shots is the difficulty in atomic force predictions. The stochastic nature of shot-based energy evaluations is incompatible with standard gradient methods. This renders the direct calculation of the analytic forces needed for MD simulations impractical in quantum hardware [58]. To circumvent this limitation while still assessing the impact of shot noise on physical properties, we employed Monte Carlo (MC) simulations, which rely only on energy evaluations. We performed canonical

MC simulations of liquid silicon at 2000 K to calculate the RDF (Figure 6). The results clearly demonstrate that the calculated RDF systematically converges to the exact result (obtained without shot noise) as the number of measurement shots increases. This confirms that accurate structural properties can be recovered, but highlights the inherent trade-off between statistical accuracy and the computational cost of the simulation.

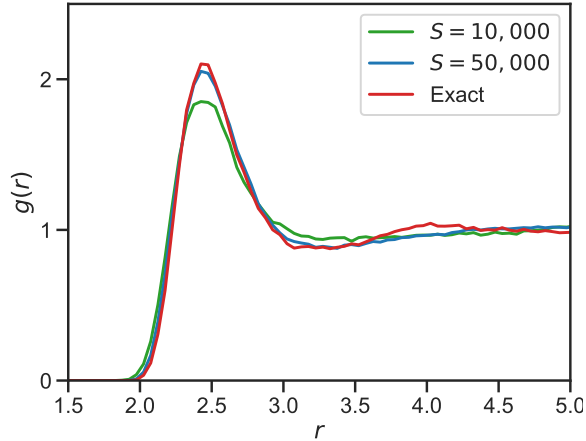


FIG. 6. Dependence of the radial distribution function of liquid silicon at  $T = 2000$  K on the number of measurement shots  $S$ . To estimate the radial distribution function, we performed canonical MC simulations.

### III.4. Conclusion

In this work, we developed and systematically evaluated a series of HQC-MLPs for the challenging task of simulating high-temperature (2000 K) liquid silicon. Our findings demonstrate that these models, which couple an  $E(3)$ -equivariant MPNN with a VQC, can accurately reproduce the underlying DFT potential energy surface. This was validated through stable canonical MD simulations, which successfully replicated key structural properties, such as the radial distribution function, in excellent agreement with our DFT reference.

Our investigation reveals a nuanced trade-off between training speed and generalization. A key advantage of the hybrid approach was a consistently accelerated convergence in training loss compared to the purely classical model. However, this was often accompanied by an earlier onset of overfitting. Crucially, we found that the model’s ability to generalize is highly sensitive to the VQC architecture, with the choice of entangling gate being paramount. The models employing controlled- $Z$  (CZ) gates consistently outperformed all other variants,

achieving the lowest validation loss and demonstrating a clear path to robust performance. This suggests that the specific nature of the entanglement operation is more critical than its mere presence.

Finally, we assessed the practical viability of these models by analyzing the impact of finite measurement shots. We confirmed that achieving chemical accuracy requires a substantial number of shots (on the order of  $10^4 - 10^5$ ) and that the resulting statistical noise makes force calculation impractical, necessitating a shift to Monte Carlo methods for simulations. Future work should therefore focus on two key areas: (1) the co-design of VQC architectures, leveraging the observed superiority of CZ-based entanglers to mitigate overfitting, and (2) the development of efficient algorithms to handle or bypass the challenges of shot noise in force estimation. By providing a detailed map of both the advantages and current hurdles, this work helps pave the way for the practical application of hybrid quantum-classical machine learning models in atomistic simulations on quantum computers.

## IV. Methods

### IV.1. Generation of training and validation datasets

The dataset used to train the machine learning potential model was generated from BOMD simulations of liquid silicon at 3000 K. This high-temperature regime was chosen to capture the complex dynamics and structural properties of liquid silicon [20], providing a challenging test case for our HQC-MLP models. The system consisted of 64 silicon atoms in a periodic simulation cell with dimensions  $10.862 \text{ \AA} \times 10.862 \text{ \AA} \times 10.862 \text{ \AA}$ . Silicon was modeled with the hybrid Gaussian and plane-wave (GPW) method [59]. Core electrons were excluded by applying norm-conserving pseudopotentials developed by Goedecker, Teter, and Hutter (GTH) [60, 61]. A charge density cutoff of 400 Ry was set for the auxiliary basis set. The Perdew-Burke-Ernzerhof (PBE) exchange-correlation functional [62] was used, and the Kohn-Sham orbitals were expanded into a double- $\zeta$  valence basis (denoted as DZVP) for the PBE functional. To ensure strict convergence of the wavefunction, the electronic gradient convergence criterion was set to  $\epsilon_{\text{SCF}} \leq 5 \times 10^{-5}$ , using the orbital transformation method to optimize single-determinant wave functions. BOMD simulations were performed using QUICKSTEP [63], which is a part of the CP2K package [64]. The nuclear equation of motion was integrated using a velocity Verlet algorithm [65] with a time step of 0.5 fs,

and a Nosé-Hoover-chain thermostat [66] was employed to regulate the temperature. These BOMD simulations generated a comprehensive set of atomic configurations, along with their corresponding energies and forces, which were crucial for training the model.

#### IV.2. Generation of models: training and optimization processes

The model architecture includes 5 interaction layers. The hidden feature dimension in each layer is represented in `e3nn` notation [32, 67] as “64x0e + 64x0o + 64x1o + 64x1e + 8x2o + 8x2e”. Radial basis vectors  $\tilde{e}_{ij}^{\text{RBF}}$  in Eq. 3 are generated using 8 radial Bessel basis functions and a polynomial envelope for the cutoff with  $p = 2$  [48]. These radial features were then input into a multilayer perceptron  $\mathcal{M}$  of size [64, 64], using SiLU nonlinearities on the outputs of the hidden layers as shown in Eq. 5. We used a cutoff of 4.5 Å, giving an average of 25 neighboring atoms per atom. The loss function used for training was

$$\mathcal{L} = \frac{1}{B} \sum_b (\hat{E}_b - E_b)^2 + \frac{\gamma_F}{3BN} \sum_{i=1}^{B \cdot N} \sum_{\alpha=1}^3 \left( -\frac{\partial \hat{E}}{\partial r_{i,\alpha}} - F_{i,\alpha} \right)^2, \quad (7)$$

where  $B$  denotes the number of batches and  $N$  the number of atoms in the batch.  $E_b$  and  $\hat{E}_b$  are the true and predicted energies for each batch, respectively,  $F_{i,\alpha}$  the force on the atom  $i$  in the direction  $\alpha \in \{x, y, z\}$ . The force loss weighting factor  $\gamma_F$  was set to 100.

The models were optimized using the AMSGRAD [68] variant of the ADAM optimizer [69] with default parameters  $\beta_1 = 0.9$ ,  $\beta_2 = 0.999$ , and  $\epsilon = 10^{-8}$ . We used a learning rate of 0.01 and a batch size of 20. The learning rate was reduced using an on-plateau scheduler based on the validation loss with a patience of 250 epochs and a decay factor of 0.9. We utilized an exponential moving average with weight 0.99 to smooth out the noisy parameter updates during training, leading to faster convergence. The models were trained with single-precision floating point format (`float32`) on an NVIDIA GeForce RTX 4090 GPU. The typical training time was approximately two days.

#### IV.3. Validation of models

**Molecular dynamics simulations:** To validate the trained HQC-MLP parameters, we performed classical isothermal ( $NVT$ ) MD simulations of liquid silicon at  $T = 2000$  K using the ASE package [70]. The integration of the equation of motion with a time step of 0.5 fs was propagated according to combined Nosé-Hoover and Parrinello-Rahman dynamics [71–73].

**Monte Carlo simulations:** To estimate stochastic potential energy under conditions relevant to real quantum computing, where atomic forces cannot be calculated, we performed Monte Carlo simulations of liquid silicon at  $T = 2000$  K. New configurations were sampled using the the Metropolis-Hastings algorithm [74].

## V. Acknowledgments

We are grateful to Luning Zhao, Joshua Goings, Torin Stetina, and Jungsang Kim for helpful discussions. CWM acknowledge the support provided by the National Research Foundation of Korea (NRF) grants funded by the Korean government (MSIT) (Grant No. RS-2023-00283929, RS-2022-NR072058). SYW and CWM acknowledge the support provided by the National Research Foundation of Korea (NRF) grants funded by the Korean government (MSIT) (Grant No. RS-2024-00407680). DCY acknowledge the support provided by the National Research Foundation of Korea (NRF) grants funded by the Korean government (MSIT) (Grant No. RS-2023-00250313). This research was supported by ‘Quantum Information Science R&D Ecosystem Creation’ through the National Research Foundation of Korea(NRF) funded by the Korean government (Ministry of Science and ICT(MSIT))(No. 2020M3H3A1110365). The authors are grateful for the computational support from the Korea Institute of Science and Technology Information (KISTI) with the NURION cluster (KSC-2023-CRE-0059, KSC-2023-CRE-0311, KSC-2023-CRE-0355, KSC-2023-CRE-0454, KSC-2023-CRE-0472, KSC-2023-CRE-0502, KSC-2024-CRE-0358,KSC-2025-CRE-0122, KSC-2025-CRE-0125). Computational work for this research was also partially performed on the OLAF supercomputer supported by IBS Research Solution Center and on the GPU cluster supported by NIPA.

## Supporting Information

Supporting Information is available for this paper.

- 
- [1] Jacob Biamonte, Peter Wittek, Nicola Pancotti, Patrick Rebentrost, Nathan Wiebe, and Seth Lloyd. Quantum machine learning. *Nature*, 549(7671):195–202, September 2017. ISSN 0028-0836, 1476-4687. doi:10.1038/nature23474.

- [2] Manas Sajjan, Junxu Li, Raja Selvarajan, Shree Hari Sureshababu, Sumit Suresh Kale, Rishabh Gupta, Vinit Singh, and Sabre Kais. Quantum machine learning for chemistry and physics. *Chem. Soc. Rev.*, 51(15):6475–6573, 2022. ISSN 0306-0012, 1460-4744. doi: 10.1039/D2CS00203E.
- [3] Kamila Zaman, Alberto Marchisio, Muhammad Abdullah Hanif, and Muhammad Shafique. A Survey on Quantum Machine Learning: Current Trends, Challenges, Opportunities, and the Road Ahead, July 2024. URL <https://arxiv.org/abs/2310.10315>.
- [4] Kamila Zaman, Tasnim Ahmed, Muhammad Abdullah Hanif, Alberto Marchisio, and Muhammad Shafique. A Comparative Analysis of Hybrid-Quantum Classical Neural Networks. In Hamid R. Arabnia, Masami Takata, Leonidas Deligiannidis, Pablo Rivas, Masahito Ohue, and Nobuaki Yasuo, editors, *Grid, Cloud, and Cluster Computing; Quantum Technologies; and Modeling, Simulation and Visualization Methods*, pages 102–115, Cham, March 2025. Springer Nature Switzerland. ISBN 978-3-031-85884-0. doi:10.1007/978-3-031-85884-0\_9.
- [5] Jules Tilly, Hongxiang Chen, Shuxiang Cao, Dario Picozzi, Kanav Setia, Ying Li, Edward Grant, Leonard Wossnig, Ivan Rungger, George H. Booth, and Jonathan Tennyson. The Variational Quantum Eigensolver: A review of methods and best practices. *Phys. Rep.*, 986: 1–128, November 2022. ISSN 03701573. doi:10.1016/j.physrep.2022.08.003.
- [6] He-Liang Huang, Xiao-Yue Xu, Chu Guo, Guojing Tian, Shi-Jie Wei, Xiaoming Sun, Wan-Su Bao, and Gui-Lu Long. Near-term quantum computing techniques: Variational quantum algorithms, error mitigation, circuit compilation, benchmarking and classical simulation. *Sci. China Phys. Mech. Astron.*, 66(5):250302, May 2023. ISSN 1674-7348, 1869-1927. doi:10.1007/s11433-022-2057-y.
- [7] Andrea Mari, Thomas R. Bromley, Josh Izaac, Maria Schuld, and Nathan Killoran. Transfer learning in hybrid classical-quantum neural networks. *Quantum*, 4:340, October 2020. ISSN 2521-327X. doi:10.22331/q-2020-10-09-340.
- [8] Joseph Bowles, Shahnawaz Ahmed, and Maria Schuld. Better than classical? The subtle art of benchmarking quantum machine learning models, March 2024. URL <https://arxiv.org/abs/2403.07059>.
- [9] Maxwell T. West, Jamie Heredge, Martin Sevier, and Muhammad Usman. Provably trainable rotationally equivariant quantum machine learning. *PRX Quantum*, 5:030320, Jul 2024. doi: 10.1103/PRXQuantum.5.030320. URL <https://link.aps.org/doi/10.1103/PRXQuantum.5.030320>.

- [10] Fabian L Thiemann, Niamh O’Neill, Venkat Kapil, Angelos Michaelides, and Christoph Schran. Introduction to machine learning potentials for atomistic simulations. *J. Phys.: Condens. Matter*, 37(7):073002, February 2025. ISSN 0953-8984. doi:10.1088/1361-648X/ad9657. URL <https://iopscience.iop.org/article/10.1088/1361-648X/ad9657>.
- [11] Abdulrahman Aldossary, Jorge Arturo Campos-Gonzalez-Angulo, Sergio Pablo-García, Shi Xuan Leong, Ella Miray Rajaonson, Luca Thiede, Gary Tom, Andrew Wang, Davide Avagliano, and Alán Aspuru-Guzik. In Silico Chemical Experiments in the Age of AI: From Quantum Chemistry to Machine Learning and Back. *Adv. Mater.*, 36(30):2402369, July 2024. ISSN 1521-4095. doi:10.1002/adma.202402369. URL <https://onlinelibrary.wiley.com/doi/abs/10.1002/adma.202402369>.
- [12] Kaiwei Wan, Jianxin He, and Xinghua Shi. Construction of High Accuracy Machine Learning Interatomic Potential for Surface/Interface of Nanomaterials—A Review. *Adv. Mater.*, 36(22):2305758, May 2024. ISSN 1521-4095. doi:10.1002/adma.202305758. URL <https://onlinelibrary.wiley.com/doi/abs/10.1002/adma.202305758>.
- [13] Emir Kocer, Tsz Wai Ko, and Jörg Behler. Neural Network Potentials: A Concise Overview of Methods. *Annu. Rev. Phys. Chem.*, 73(1):163–186, April 2022. doi:10.1146/annurev-physchem-082720-034254. URL <https://www.annualreviews.org/doi/abs/10.1146/annurev-physchem-082720-034254>.
- [14] Oliver T. Unke, Stefan Chmiela, Huziel E. Sauceda, Michael Gastegger, Igor Poltavsky, Kristof T. Schütt, Alexandre Tkatchenko, and Klaus-Robert Müller. Machine Learning Force Fields. *Chem. Rev.*, 121(16):10142–10186, August 2021. ISSN 0009-2665, 1520-6890. doi:10.1021/acs.chemrev.0c01111.
- [15] Jörg Behler. Four Generations of High-Dimensional Neural Network Potentials. *Chem. Rev.*, 121(16):10037–10072, August 2021. ISSN 0009-2665. doi:10.1021/acs.chemrev.0c00868. URL <https://pubs.acs.org/doi/10.1021/acs.chemrev.0c00868>.
- [16] Pavlo O. Dral. Quantum Chemistry in the Age of Machine Learning. *J. Phys. Chem. Lett.*, 11(6):2336–2347, March 2020. doi:10.1021/acs.jpcllett.9b03664. URL <https://doi.org/10.1021/acs.jpcllett.9b03664>.
- [17] Amil Merchant, Simon Batzner, Samuel S. Schoenholz, Muratahan Aykol, Gowoon Cheon, and Ekin Dogus Cubuk. Scaling deep learning for materials discovery. *Nature*, 624(7990):80–85, December 2023. ISSN 0028-0836, 1476-4687. doi:10.1038/s41586-023-06735-9.

- [18] Ilyes Batatia, Philipp Benner, Yuan Chiang, Alin M. Elena, Dávid P. Kovács, Janosh Riebesell, Xavier R. Advincula, Mark Asta, Matthew Avaylon, William J. Baldwin, Fabian Berger, Noam Bernstein, Arghya Bhowmik, Samuel M. Blau, Vlad Cărare, James P. Darby, Sandip De, Flaviano Della Pia, Volker L. Deringer, Rokas Elijošius, Zakariya El-Machachi, Fabio Falcioni, Edvin Fako, Andrea C. Ferrari, Annalena Genreith-Schriever, Janine George, Rhys E. A. Goodall, Clare P. Grey, Petr Grigorev, Shuang Han, Will Handley, Hendrik H. Heenen, Kersti Hermansson, Christian Holm, Jad Jaafar, Stephan Hofmann, Konstantin S. Jakob, Hyunwook Jung, Venkat Kapil, Aaron D. Kaplan, Nima Karimitari, James R. Kermode, Namu Kroupa, Jolla Kullgren, Matthew C. Kuner, Domantas Kuryla, Guoda Liepuoniute, Johannes T. Margraf, Ioan-Bogdan Magdău, Angelos Michaelides, J. Harry Moore, Aakash A. Naik, Samuel P. Niblett, Sam Walton Norwood, Niamh O’Neill, Christoph Ortner, Kristin A. Persson, Karsten Reuter, Andrew S. Rosen, Lars L. Schaaf, Christoph Schran, Benjamin X. Shi, Eric Sivonxay, Tamás K. Stenczel, Viktor Svahn, Christopher Sutton, Thomas D. Swinburne, Jules Tilly, Cas van der Oord, Eszter Varga-Umbrich, Tejs Vegge, Martin Vondrák, Yangshuai Wang, William C. Witt, Fabian Zills, and Gábor Csányi. A foundation model for atomistic materials chemistry, March 2024. URL <https://arxiv.org/abs/2401.00096>.
- [19] Chang Woo Myung, Amir Hajibabaei, Ji-Hyun Cha, Miran Ha, Junu Kim, and Kwang S. Kim. Challenges, Opportunities, and Prospects in Metal Halide Perovskites from Theoretical and Machine Learning Perspectives. *Adv. Energy Mater.*, 12(45):2202279, December 2022. ISSN 1614-6832, 1614-6840. doi:10.1002/aenm.202202279.
- [20] Jörg Behler and Michele Parrinello. Generalized Neural-Network Representation of High-Dimensional Potential-Energy Surfaces. *Phys. Rev. Lett.*, 98(14):146401, April 2007. ISSN 0031-9007, 1079-7114. doi:10.1103/PhysRevLett.98.146401.
- [21] Marco Eckhoff and Jörg Behler. High-dimensional neural network potentials for magnetic systems using spin-dependent atom-centered symmetry functions. *npj Comput. Mater.*, 7(1):170, December 2021. ISSN 2057-3960. doi:10.1038/s41524-021-00636-z.
- [22] Albert P. Bartók, Mike C. Payne, Risi Kondor, and Gábor Csányi. Gaussian Approximation Potentials: The Accuracy of Quantum Mechanics, without the Electrons. *Phys. Rev. Lett.*, 104(13):136403, April 2010. ISSN 0031-9007, 1079-7114. doi:10.1103/PhysRevLett.104.136403.
- [23] Albert P. Bartók, Risi Kondor, and Gábor Csányi. On representing chemical environments. *Phys. Rev. B*, 87(18):184115, May 2013. ISSN 1098-0121, 1550-235X. doi:10.1103/PhysRevB.87.184115.

- [24] Albert P. Bartók and Gábor Csányi. Gaussian approximation potentials: A brief tutorial introduction. *Int. J. Quantum Chem.*, 115(16):1051–1057, August 2015. ISSN 1097-461X. doi:10.1002/qua.24927. URL <https://onlinelibrary.wiley.com/doi/10.1002/qua.24927>.
- [25] Sascha Klawohn, James P. Darby, James R. Kermode, Gábor Csányi, Miguel A. Caro, and Albert P. Bartók. Gaussian approximation potentials: Theory, software implementation and application examples. *J. Chem. Phys.*, 159(17):174108, November 2023. ISSN 0021-9606, 1089-7690. doi:10.1063/5.0160898.
- [26] Amir Hajibabaei, Miran Ha, Saeed Pourasad, Junu Kim, and Kwang S. Kim. Machine Learning of First-Principles Force-Fields for Alkane and Polyene Hydrocarbons. *J. Phys. Chem. A*, 125(42):9414–9420, October 2021. ISSN 1089-5639, 1520-5215. doi:10.1021/acs.jpca.1c05819.
- [27] Amir Hajibabaei, Chang Woo Myung, and Kwang S. Kim. Sparse Gaussian process potentials: Application to lithium diffusivity in superionic conducting solid electrolytes. *Phys. Rev. B*, 103(21):214102, June 2021. ISSN 2469-9950, 2469-9969. doi:10.1103/PhysRevB.103.214102.
- [28] Amir Hajibabaei and Kwang S. Kim. Universal Machine Learning Interatomic Potentials: Surveying Solid Electrolytes. *J. Phys. Chem. Lett.*, 12(33):8115–8120, August 2021. ISSN 1948-7185, 1948-7185. doi:10.1021/acs.jpcclett.1c01605.
- [29] Miran Ha, Amir Hajibabaei, Saeed Pourasad, and Kwang S. Kim. Sparse Gaussian Process Regression-Based Machine Learned First-Principles Force-Fields for Saturated, Olefinic, and Aromatic Hydrocarbons. *ACS Phys. Chem Au*, 2(3):260–264, May 2022. ISSN 2694-2445, 2694-2445. doi:10.1021/acspchemau.1c00058.
- [30] Soohaeng Yoo Willow, Dong Geon Kim, R. Sundheep, Amir Hajibabaei, Kwang S. Kim, and Chang Woo Myung. Active sparse Bayesian committee machine potential for isothermal–isobaric molecular dynamics simulations. *Phys. Chem. Chem. Phys.*, 26(33):22073–22082, 2024. ISSN 1463-9076, 1463-9084. doi:10.1039/D4CP01801J.
- [31] Joaquin Quiñonero-Candela and Carl Edward Rasmussen. A Unifying View of Sparse Approximate Gaussian Process Regression. *J. Mach. Learn. Res.*, 6(65):1939–1959, 2005.
- [32] Mario Geiger and Tess Smidt. e3nn: Euclidean neural networks. *arXiv e-prints*, page arXiv:2207.09453, 2022. URL <https://arxiv.org/abs/2207.09453>.
- [33] Simon Batzner, Albert Musaelian, Lixin Sun, Mario Geiger, Jonathan P. Mailoa, Mordechai Kornbluth, Nicola Molinari, Tess E. Smidt, and Boris Kozinsky. E(3)-equivariant graph neural networks for data-efficient and accurate interatomic potentials. *Nat. Commun.*, 13(1):2453, May 2022. ISSN 2041-1723. doi:10.1038/s41467-022-29939-5.

- [34] Taco S. Cohen, Mario Geiger, and Maurice Weiler. A general theory of equivariant CNNs on homogeneous spaces. In *Proceedings of the 33rd International Conference on Neural Information Processing Systems*, NIPS '19, pages 9145–9156, Red Hook, NY, USA, December 2019. Curran Associates Inc. doi: 10.5555/3454287.3455107. URL <https://dl.acm.org/doi/10.5555/3454287.3455107>. [https://papers.nips.cc/paper\\_files/paper/2019/hash/b9cfe8b6042cf759dc4c0cccb27a6737-Abstract.html](https://papers.nips.cc/paper_files/paper/2019/hash/b9cfe8b6042cf759dc4c0cccb27a6737-Abstract.html).
- [35] Taco Cohen, Maurice Weiler, Berkay Kicanaoglu, and Max Welling. Gauge Equivariant Convolutional Networks and the Icosahedral CNN. In *Proceedings of the 36th International Conference on Machine Learning*, volume 97, pages 1321–1330, Long Beach, CA, USA, May 2019. ML Research Press. URL <https://proceedings.mlr.press/v97/cohen19d.html>. ISSN: 2640-3498.
- [36] M. Cerezo, Guillaume Verdon, Hsin-Yuan Huang, Lukasz Cincio, and Patrick J. Coles. Challenges and opportunities in quantum machine learning. *Nat. Comput. Sci.*, 2(9):567–576, September 2022. ISSN 2662-8457. doi:10.1038/s43588-022-00311-3. URL <https://doi.org/10.1038/s43588-022-00311-3>.
- [37] Tomoya Shiota, Kenji Ishihara, and Wataru Mizukami. Universal neural network potentials as descriptors: towards scalable chemical property prediction using quantum and classical computers. *Digit. Discov.*, 3(9):1714–1728, September 2024. ISSN 2635-098X. doi: 10.1039/D4DD00098F. URL <https://pubs.rsc.org/en/content/articlelanding/2024/dd/d4dd00098f>.
- [38] Yannick Couzinié, Shunsuke Daimon, Hirofumi Nishi, Natsuki Ito, Yusuke Harazono, and Yuichiro Matsushita. Towards Improved Quantum Machine Learning for Molecular Force Fields, May 2025. URL <https://arxiv.org/abs/2505.03213>.
- [39] François Le Gall. Robust Dequantization of the Quantum Singular Value Transformation and Quantum Machine Learning Algorithms. *comput. complex.*, 34(1):2, January 2025. ISSN 1420-8954. doi:10.1007/s00037-024-00262-3. URL <https://link.springer.com/article/10.1007/s00037-024-00262-3>.
- [40] Nai-Hui Chia, András Gilyén, Tongyang Li, Han-Hsuan Lin, Ewin Tang, and Chunhao Wang. Sampling-based sublinear low-rank matrix arithmetic framework for dequantizing Quantum machine learning. In *Proceedings of the 52nd Annual ACM SIGACT Symposium on Theory of Computing*, pages 387–400, Chicago IL USA, June 2020. ACM. ISBN 978-1-4503-6979-4.

- doi:10.1145/3357713.3384314. URL <https://dl.acm.org/doi/10.1145/3357713.3384314>.
- [41] Ryan Babbush, Jarrod R. McClean, Michael Newman, Craig Gidney, Sergio Boixo, and Hartmut Neven. Focus beyond Quadratic Speedups for Error-Corrected Quantum Advantage. *PRX Quantum*, 2(1):010103, March 2021. ISSN 2691-3399. doi:10.1103/PRXQuantum.2.010103. URL <https://link.aps.org/doi/10.1103/PRXQuantum.2.010103>.
- [42] Lov K. Grover. A fast quantum mechanical algorithm for database search. In *Proceedings of the twenty-eighth annual ACM symposium on Theory of computing - STOC '96*, pages 212–219, Philadelphia, Pennsylvania, United States, 1996. ACM Press. ISBN 978-0-89791-785-8. doi:10.1145/237814.237866. URL <http://portal.acm.org/citation.cfm?doid=237814.237866>.
- [43] Ethan Bernstein and Umesh Vazirani. Quantum complexity theory. *SIAM Journal on Computing*, 26(5):1411–1473, 1997. doi:10.1137/S0097539796300921. URL <https://doi.org/10.1137/S0097539796300921>.
- [44] Wei Zi, Siyi Wang, Hyunji Kim, Xiaoming Sun, Anupam Chattopadhyay, and Patrick Rebentrost. Efficient quantum circuits for machine learning activation functions including constant T-depth ReLU. 6(4):043048, October 2024. doi:10.1103/PhysRevResearch.6.043048. URL <https://journals.aps.org/prresearch/abstract/10.1103/PhysRevResearch.6.043048>.
- [45] Frank H. Stillinger and Thomas A. Weber. Computer simulation of local order in condensed phases of silicon. *Phys. Rev. B*, 31(8):5262–5271, April 1985. doi:10.1103/PhysRevB.31.5262. URL <https://link.aps.org/doi/10.1103/PhysRevB.31.5262>.
- [46] Thomas J Lenosky, Babak Sadigh, Eduardo Alonso, Vasily V Bulatov, Tomas Diaz de la Rubia, Jeongnim Kim, Arthur F Voter, and Joel D Kress. Highly optimized empirical potential model of silicon. *Model. Simul. Mater. Sci. Eng.*, 8(6):825, nov 2000. doi:10.1088/0965-0393/8/6/305. URL <https://dx.doi.org/10.1088/0965-0393/8/6/305>.
- [47] Shiliang Zhang, Li-Min Wang, Xinyu Zhang, Li Qi, Suhong Zhang, Mingzhen Ma, and Riping Liu. Polymorphism in glassy silicon: Inherited from liquid-liquid phase transition in supercooled liquid. *Sci. Rep.*, 5(1):8590, February 2015. ISSN 2045-2322. doi:10.1038/srep08590. URL <https://www.nature.com/articles/srep08590>.
- [48] Johannes Gasteiger, Chandan Yeshwanth, and Stephan Günnemann. Directional Message Passing on Molecular Graphs via Synthetic Coordinates. In *Advances in Neural Information Processing Systems*, volume 34, pages 15421–15433. Curran Associates, Inc., December 2021. URL <https://proceedings.neurips.cc/paper/2021/hash/82489c9737cc245530c7a6ebef3753ec-Abstract.html>.

- [49] Kaiming He, Xiangyu Zhang, Shaoqing Ren, and Jian Sun. Deep Residual Learning for Image Recognition. In *Proceedings of the IEEE Conference on Computer Vision and Pattern Recognition*, volume 2016, pages 770–778, June 2016. URL [https://openaccess.thecvf.com/content\\_cvpr\\_2016/html/He\\_Deep\\_Residual\\_Learning\\_CVPR\\_2016\\_paper.html](https://openaccess.thecvf.com/content_cvpr_2016/html/He_Deep_Residual_Learning_CVPR_2016_paper.html).
- [50] Ville Bergholm, Josh Izaac, Maria Schuld, Christian Gogolin, Shah Nawaz Ahmed, Vishnu Ajith, M. Sohaib Alam, Guillermo Alonso-Linaje, B. Akash Narayanan, Ali Asadi, Juan Miguel Arrazola, Utkarsh Azad, Sam Banning, Carsten Blank, Thomas R. Bromley, Benjamin A. Cordier, Jack Ceroni, Alain Delgado, Olivia Di Matteo, Amintor Dusko, Tanya Garg, Diego Guala, Anthony Hayes, Ryan Hill, Aroosa Ijaz, Theodor Isacsson, David Ittah, Soran Jangiri, Prateek Jain, Edward Jiang, Ankit Khandelwal, Korbinian Kottmann, Robert A. Lang, Christina Lee, Thomas Loke, Angus Lowe, Keri McKiernan, Johannes Jakob Meyer, J. A. Montañez-Barrera, Romain Moyard, Zeyue Niu, Lee James O’Riordan, Steven Oud, Ashish Panigrahi, Chae-Yeun Park, Daniel Polatajko, Nicolás Quesada, Chase Roberts, Nahum Sá, Isidor Schoch, Borun Shi, Shuli Shu, Sukin Sim, Arshpreet Singh, Ingrid Strandberg, Jay Soni, Antal Száva, Slimane Thabet, Rodrigo A. Vargas-Hernández, Trevor Vincent, Nicola Vitucci, Maurice Weber, David Wierichs, Roeland Wiersema, Moritz Willmann, Vincent Wong, Shaoming Zhang, and Nathan Killoran. PennyLane: Automatic differentiation of hybrid quantum-classical computations, July 2022.
- [51] Jarrod R. McClean, Sergio Boixo, Vadim N. Smelyanskiy, Ryan Babbush, and Hartmut Neven. Barren plateaus in quantum neural network training landscapes. *Nat. Commun.*, 9(1):4812, November 2018. ISSN 2041-1723. doi:10.1038/s41467-018-07090-4. URL <https://www.nature.com/articles/s41467-018-07090-4>.
- [52] Zoë Holmes, Kunal Sharma, M. Cerezo, and Patrick J. Coles. Connecting ansatz expressibility to gradient magnitudes and barren plateaus. *PRX Quantum*, 3:010313, Jan 2022. doi:10.1103/PRXQuantum.3.010313. URL <https://link.aps.org/doi/10.1103/PRXQuantum.3.010313>.
- [53] M. Cerezo, Akira Sone, Tyler Volkoff, Lukasz Cincio, and Patrick J. Coles. Cost function dependent barren plateaus in shallow parametrized quantum circuits. *Nat. Commun.*, 12(1):1791, March 2021. ISSN 2041-1723. doi:10.1038/s41467-021-21728-w. URL <https://www.nature.com/articles/s41467-021-21728-w>.
- [54] Kunal Sharma, M. Cerezo, Lukasz Cincio, and Patrick J. Coles. Trainability of dissipative perceptron-based quantum neural networks. *Phys. Rev. Lett.*, 128:180505, May 2022. doi:

- 10.1103/PhysRevLett.128.180505. URL <https://link.aps.org/doi/10.1103/PhysRevLett.128.180505>.
- [55] Taylor L. Patti, Khadijeh Najafi, Xun Gao, and Susanne F. Yelin. Entanglement devised barren plateau mitigation. *Phys. Rev. Res.*, 3(3):033090, July 2021. ISSN 2643-1564. doi:10.1103/PhysRevResearch.3.033090. URL <https://link.aps.org/doi/10.1103/PhysRevResearch.3.033090>.
- [56] Martin Z. Bazant, Efthimios Kaxiras, and J. F. Justo. Environment-dependent interatomic potential for bulk silicon. *Phys. Rev. B*, 56:8542–8552, Oct 1997. doi:10.1103/PhysRevB.56.8542. URL <https://link.aps.org/doi/10.1103/PhysRevB.56.8542>.
- [57] J. Tersoff. Empirical interatomic potential for silicon with improved elastic properties. *Phys. Rev. B*, 38:9902–9905, Nov 1988. doi:10.1103/PhysRevB.38.9902. URL <https://link.aps.org/doi/10.1103/PhysRevB.38.9902>.
- [58] Thomas E. O’Brien, Michael Streif, Nicholas C. Rubin, Raffaele Santagati, Yuan Su, William J. Huggins, Joshua J. Goings, Nikolaj Moll, Elica Kyoseva, Matthias Degroote, Christofer S. Tautermann, Joonho Lee, Dominic W. Berry, Nathan Wiebe, and Ryan Babbush. Efficient quantum computation of molecular forces and other energy gradients. *Phys. Rev. Res.*, 4(4):043210, December 2022. doi:10.1103/PhysRevResearch.4.043210. URL <https://link.aps.org/doi/10.1103/PhysRevResearch.4.043210>.
- [59] GERALD Lippert, JURG Hutter, and MICHELE Parrinello. A hybrid gaussian and plane wave density functional scheme. *Mol. Phys.*, 92(3):477–488, 1997. doi:10.1080/002689797170220.
- [60] S. Goedecker, M. Teter, and J. Hutter. Separable dual-space gaussian pseudopotentials. *Phys. Rev. B*, 54:1703–1710, Jul 1996. doi:10.1103/PhysRevB.54.1703. URL <https://link.aps.org/doi/10.1103/PhysRevB.54.1703>.
- [61] C. Hartwigsen, S. Goedecker, and J. Hutter. Relativistic separable dual-space gaussian pseudopotentials from h to rn. *Phys. Rev. B*, 58:3641–3662, Aug 1998. doi:10.1103/PhysRevB.58.3641. URL <https://link.aps.org/doi/10.1103/PhysRevB.58.3641>.
- [62] John P. Perdew, Kieron Burke, and Matthias Ernzerhof. Generalized gradient approximation made simple. *Phys. Rev. Lett.*, 77:3865–3868, Oct 1996. doi:10.1103/PhysRevLett.77.3865. URL <https://link.aps.org/doi/10.1103/PhysRevLett.77.3865>.
- [63] Joost VandeVondele, Matthias Krack, Fawzi Mohamed, Michele Parrinello, Thomas Chassaing, and Jürg Hutter. Quickstep: Fast and accurate density functional calculations using a mixed gaussian and plane waves approach. *Comput. Phys. Commun.*, 167(2):103–

- 128, 2005. ISSN 0010-4655. doi:<https://doi.org/10.1016/j.cpc.2004.12.014>. URL <https://www.sciencedirect.com/science/article/pii/S0010465505000615>.
- [64] Thomas D. Kühne, Marcella Iannuzzi, Mauro Del Ben, Vladimir V. Rybkin, Patrick Seewald, Frederick Stein, Teodoro Laino, Rustam Z. Khaliullin, Ole Schütt, Florian Schiffmann, Dorothea Golze, Jan Wilhelm, Sergey Chulkov, Mohammad Hossein Bani-Hashemian, Valéry Weber, Urban Borštnik, Mathieu Taillefumier, Alice Shoshana Jakobovits, Alfio Lazzaro, Hans Pabst, Tiziano Müller, Robert Schade, Manuel Guidon, Samuel Andermatt, Nico Holmberg, Gregory K. Schenter, Anna Hehn, Augustin Bussy, Fabian Belleflamme, Gloria Tabacchi, Andreas Glöß, Michael Lass, Iain Bethune, Christopher J. Mundy, Christian Pleschl, Matt Watkins, Joost VandeVondele, Matthias Krack, and Jürg Hutter. CP2K: An electronic structure and molecular dynamics software package - Quickstep: Efficient and accurate electronic structure calculations. *J. Chem. Phys.*, 152(19):194103, 05 2020. ISSN 0021-9606. doi:10.1063/5.0007045. URL <https://doi.org/10.1063/5.0007045>.
- [65] William C. Swope, Hans C. Andersen, Peter H. Berens, and Kent R. Wilson. A computer simulation method for the calculation of equilibrium constants for the formation of physical clusters of molecules: Application to small water clusters. *J. Chem. Phys.*, 76(1):637–649, 01 1982. ISSN 0021-9606. doi:10.1063/1.442716. URL <https://doi.org/10.1063/1.442716>.
- [66] Glenn J. Martyna, Michael L. Klein, and Mark Tuckerman. Nosé–Hoover chains: The canonical ensemble via continuous dynamics. *J. Chem. Phys.*, 97(4):2635–2643, 08 1992. ISSN 0021-9606. doi:10.1063/1.463940. URL <https://doi.org/10.1063/1.463940>.
- [67] Mario Geiger, Tess Smidt, Alby M., Benjamin Kurt Miller, Wouter Boomsma, Bradley Dice, Kostiantyn Lapchevskyi, Maurice Weiler, Michał Tyszkiewicz, Simon Batzner, Dylan Madisetti, Martin Uhrin, Jes Frellsen, Nuri Jung, Sophia Sanborn, Mingjian Wen, Josh Rackers, Marcel Rød, and Michael Bailey. Euclidean neural networks: e3nn, April 2022. URL <https://doi.org/10.5281/zenodo.6459381>.
- [68] Sashank J. Reddi, Satyen Kale, and Sanjiv Kumar. On the Convergence of Adam and Beyond. In *Proceedings of the 6th International Conference on Learning Representations*, Vancouver, BC, Canada, February 2018. OpenReview. URL <https://openreview.net/forum?id=ryQu7f-RZ>. <https://openreview.net/group?id=ICLR.cc/2018/Conference>.
- [69] Diederik P. Kingma and Jimmy Ba. Adam: A Method for Stochastic Optimization, January 2017. URL <https://arxiv.org/abs/1412.6980>.

- [70] Ask Hjorth Larsen, Jens Jørgen Mortensen, Jakob Blomqvist, Ivano E. Castelli, Rune Christensen, Marcin Dułak, Jesper Friis, Michael N. Groves, Bjørk Hammer, Cory Hargus, Eric D. Hermes, Paul C. Jennings, Peter Bjerre Jensen, James Kermode, John R. Kitchin, Esben Leonhard Kolsbjerg, Joseph Kubal, Kristen Kaasbjerg, Steen Lysgaard, Jón Bergmann Maronsson, Tristan Maxson, Thomas Olsen, Lars Pastewka, Andrew Peterson, Carsten Rostgaard, Jakob Schiøtz, Ole Schütt, Mikkel Strange, Kristian S. Thygesen, Tejs Vegge, Lasse Vilhelmsen, Michael Walter, Zhenhua Zeng, and Karsten W. Jacobsen. The atomic simulation environment—a Python library for working with atoms. *J. Phys. Condens. Matter*, 29(27):273002, June 2017. ISSN 0953-8984. doi:10.1088/1361-648X/aa680e. URL <https://dx.doi.org/10.1088/1361-648X/aa680e>. Publisher: IOP Publishing.
- [71] Simone Melchionna, Giovanni Ciccotti, and Brad L. Holian. Hoover NPT dynamics for systems varying in shape and size. *Mol. Phys.*, 78:533–544, 1993.
- [72] Simone Melchionna. Constrained systems and statistical distribution. *Phys. Rev. E*, 61(6):6165–6170, June 2000. ISSN 1063-651X, 1095-3787. doi:10.1103/PhysRevE.61.6165.
- [73] Brad Lee Holian, Anthony J. De Groot, William G. Hoover, and Carol G. Hoover. Time-reversible equilibrium and nonequilibrium isothermal-isobaric simulations with centered-difference Stoermer algorithms. *Phys. Rev. A*, 41(8):4552–4553, April 1990. ISSN 1050-2947, 1094-1622. doi:10.1103/PhysRevA.41.4552.
- [74] W. K. Hastings. Monte carlo sampling methods using markov chains and their applications. *Biometrika*, 57(1):97–109, 04 1970. ISSN 0006-3444. doi:10.1093/biomet/57.1.97. URL <https://doi.org/10.1093/biomet/57.1.97>.

# Electronic Supplementary Information: Hybrid Quantum–Classical Machine Learning Potential with Variational Quantum Circuits

Soohaeng Yoo Willow,<sup>1</sup> David ChangMo Yang,<sup>1</sup> and Chang Woo Myung<sup>1,2,3,\*</sup>

<sup>1</sup>*Department of Energy Science, Sungkyunkwan University,  
Seobu-ro 2066, Suwon, 16419, Korea*

<sup>2</sup>*Department of Energy, Sungkyunkwan University,  
Seobu-ro 2066, Suwon, 16419, Korea*

<sup>3</sup>*Department of Quantum Information Engineering,  
Sungkyunkwan University, Seobu-ro 2066, Suwon, 16419, Korea*

(Dated: August 7, 2025)

---

\* [cwmyung@skku.edu](mailto:cwmyung@skku.edu)

## S1. Rotationally equivariant tensor product

The tensor product  $\otimes$  in the interatomic continuous-filter convolution  $f_{\text{Conv}}$  is given by:

$$[e_{ij}]_{m_e}^{l_e} \otimes [h_j]_{m_h}^{l_h} = \sum_{m_e, m_h} C_{l_h, m_h, l_e, m_e}^{l_o, m_o} [e_{ij}]_{m_e}^{l_e} [h_j]_{m_h}^{l_h} \rightarrow [O_{ij}]_{m_o}^{l_o}, \quad (\text{S1})$$

where “rotational order”  $l = 0, 1, 2, \dots$  is a non-negative integer. The representation index  $m$  takes values  $m \in [-l, l]$ .  $C$  indicates the Clebsch-Gordan coefficients.

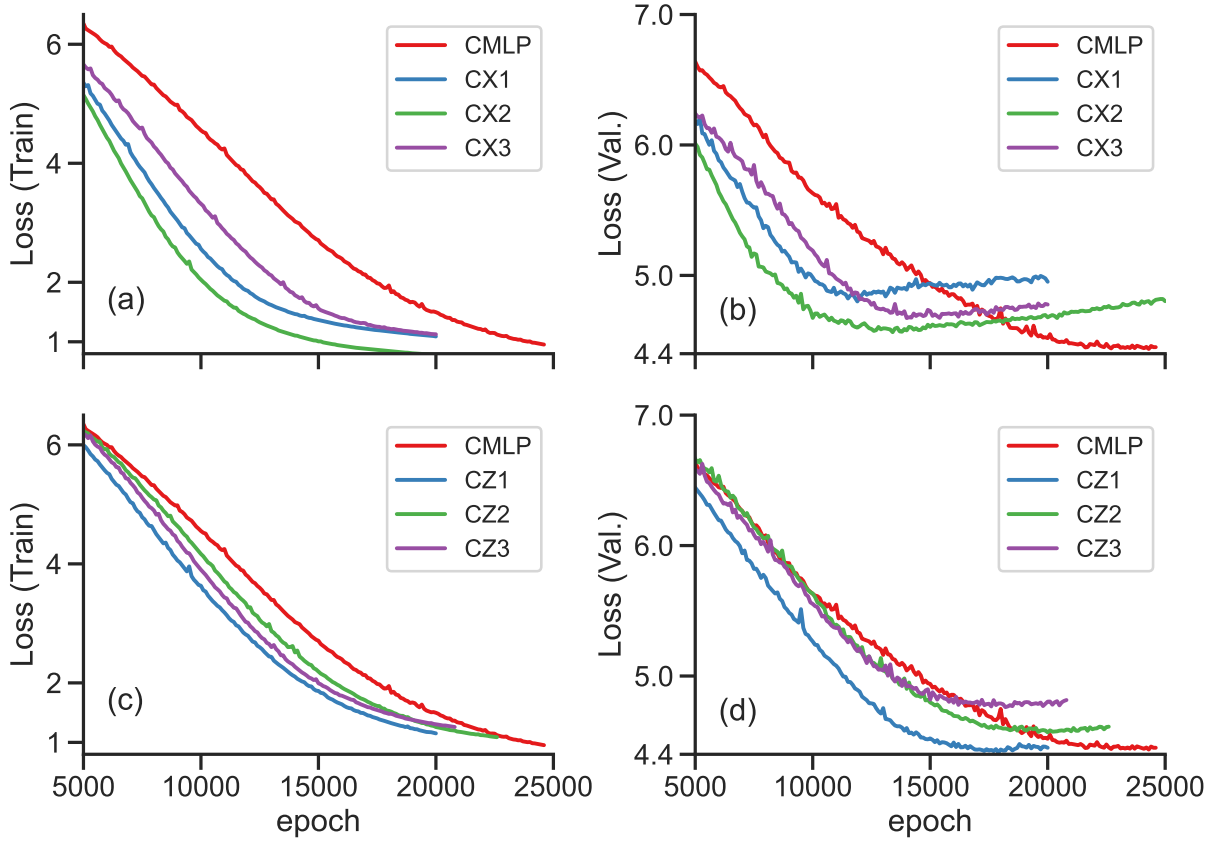


FIG. S1. The loss profiles of hybrid quantum-classical machine learning potential (HQC-MLP) models with `BasicEntanglerCX` and `BasicEntanglerCZ` Ansatz modules compared to a classical machine learning potential (CMLP). Panels (a) and (b) show training and validation losses, respectively, for the `BasicEntanglerCX` Ansatz with three different random seeds (CX1, CX2, CX3). Panels (c) and (d) show corresponding results for the `BasicEntanglerCZ` Ansatz (CZ1, CZ2, CZ3). In the validation datasets, the loss values exhibit clear minima, indicating the onset of overfitting as training progresses.

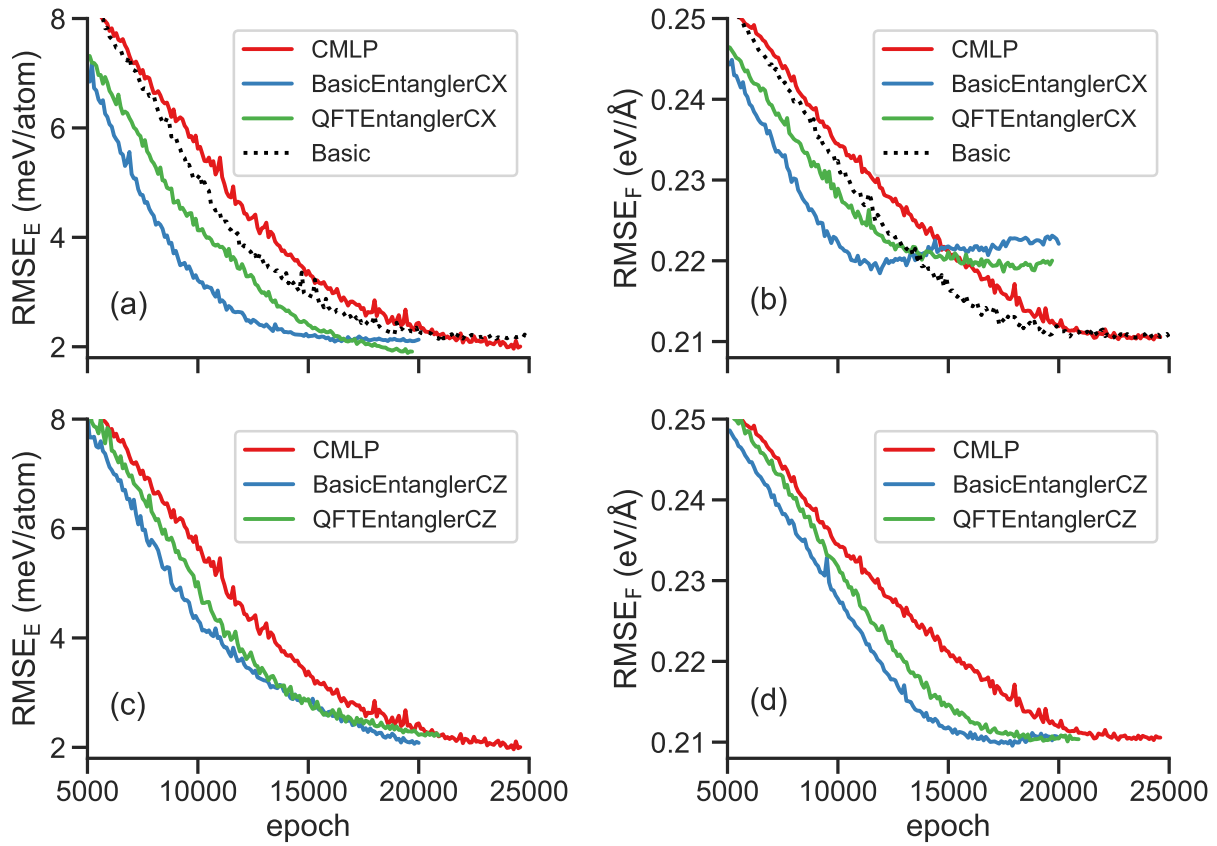


FIG. S2. The root mean squared errors (RMSEs) for predicted energies per atom ( $\text{RMSE}_E$ ) and predicted forces ( $\text{RMSE}_F$ ) are shown using the test dataset. The HQC-MLP model (blue dashed lines) shows a faster decrease in both  $\text{RMSE}_E$  and  $\text{RMSE}_F$  compared to the CMLP model (red lines). Despite some overfitting in HQC-MLP model, both models produced similar values:  $\text{RMSE}_E \approx 2.0$  meV/atom and  $\text{RMSE}_F \approx 0.21 \sim 0.22$  eV/Å.

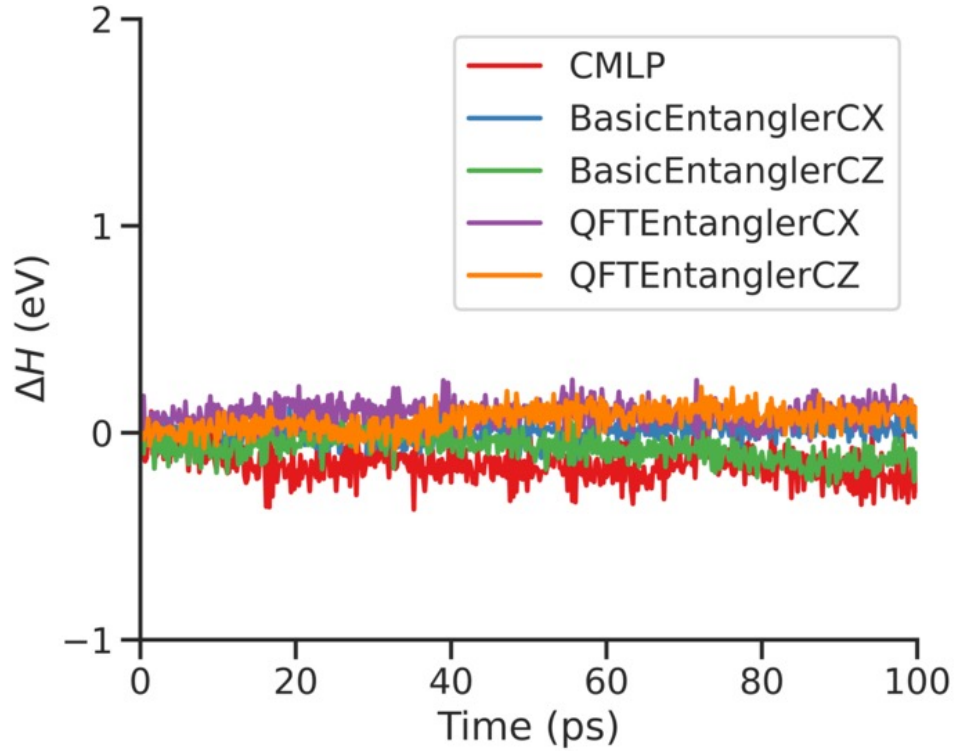


FIG. S3. Conservation of the Hamiltonian. Canonical molecular dynamics simulations were carried out at a temperature of  $T = 2000$  K using machine learning potential models. The relative Hamiltonian, denoted as  $\Delta H$ , is defined by the expression  $\Delta H = H(t) - H(t = 0)$ , where  $H(t)$  represents the Hamiltonian at time  $t$  and  $H(0)$  is the initial Hamiltonian.

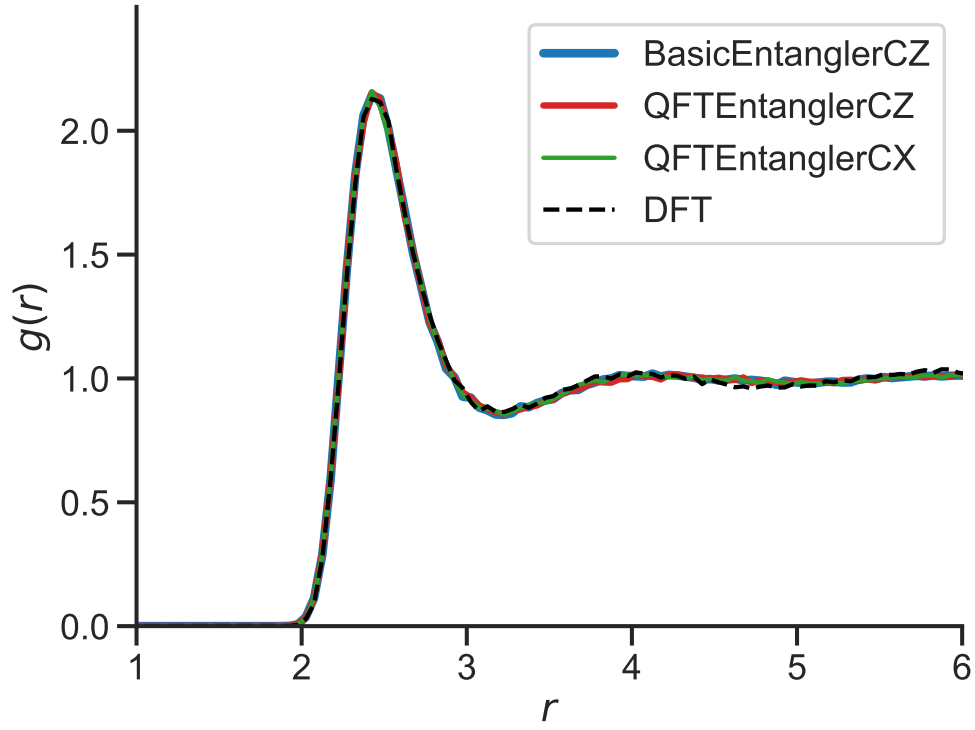


FIG. S4. Radial distribution function,  $g(r)$ , for liquid silicon at  $T = 2000$  K. The plot compares the results from the HQC-MLP (BasicEntanglerCZ, QFTEntanglerCZ, and QFTEntanglerCX) with the reference calculated using DFT (dashed black line), demonstrating excellent agreement.